1956-05

Description of a counter experiment to measure the elastic proton-proton scattering cross section at bevatron energies.

Causey, Charles Wesley

Monterey, California. Naval Postgraduate School

DESCRIPTION OF A COUNTER EXPERIMENT TO MEASURE THE ELASTIC PROTON-PROTON SCATTERING CROSS SECTION AT BEVATRON ENERGIES

Charles Wesley Causey

1-29

BEV - BEVATRON
ENE - ENERGIES
PRP - PROTON

Letter on cover:

DESCRIPTION OF A COUNTER
EXPERIMENT TO MEASURE THE ELASTIC
PROTON-PROTON SCATTERING CROSS
SECTION AT BEVATRON ENERGIES

Charles Wesley Causey

UCRL-3413

UNIVERSITY OF CALIFORNIA

Radiation Laboratory
Berkeley, California

Contract No. W-7405-eng-48

DESCRIPTION OF A COUNTER EXPERIMENT TO MEASURE THE ELASTIC PROTON-PROTON SCATTERING CROSS SECTION AT BEVATRON ENERGIES

Charles Wesley Causey

(M. S. Thesis)

May 14, 1956

Submitted in partial fulfillment
of the requirements for the degree of

MASTER OF SCIENCE
in
PHYSICS

United States Naval Postgraduate School
Monterey, California

Printed for the U. S. Atomic Energy Commission

This work is accepted as fulfilling

the thesis requirements for the degree of

MASTER OF SCIENCE

IN

PHYSICS

from the

United States Naval Postgraduate School

DESCRIPTION OF A COUNTER EXPERIMENT TO MEASURE THE ELASTIC PROTON-PROTON SCATTERING CROSS SECTION AT BEVATRON ENERGIES

Charles Wesley Causey

Radiation Laboratory
University of California
Berkeley, California

May 14, 1956

ABSTRACT

The differential cross section for proton-proton elastic scattering has been measured as a function of angle at the Bevatron at energies of 0.92, 2.24, 3.49, 4.40, and 6.2 Bev by Bruce Cork, William A. Wenzel, and Charles W. Causey. At each energy, measurements were made out to the largest center-of-mass angle at which the scattering cross section was still detectable. At 2.24, 4.40, and 6.2 Bev measurements were made in to the smallest laboratory angle possible at which the recoil proton of the lower energy was still detectable. These smallest practicable laboratory angles were equivalent to 14.8° (center of mass) at 2.24 Bev, 11° (c.m.) at 4.40 Bev, and 8.3° (c.m.) at 6.2 Bev. The counters and electronics used are described, and some results are presented.

PREFACE

One of the measurements of interest in the investigation of nuclear forces is the cross section for proton-proton elastic scattering. This cross section at lower energies provides information on the nuclear forces at ranges where the nuclear forces are attractive. At energies higher than 40 Mev the cross sections yield information on the nature of the strong repulsive forces that must exist at very short internuclear ranges.

When the kinetic energy of the bombarding proton is increased to energies above several hundred million electron volts, reactions other than elastic proton-proton scattering can occur. At about 290 Mev the production of π mesons becomes possible; at ~ 1.15 Bev, K- and τ-meson production can take place; and the antinucleon production threshold is ~ 5.6 Bev. The measurement experiment must thus be designed to distinguish between protons scattered from elastic collisions and the protons, mesons, and antinucleons scattered from inelastic events.

It is the purpose of this paper to describe the manner in which the elastic proton-proton cross-section measurement was performed at Bevatron energies by Bruce Cork, William A. Wenzel, and the writer. The complete results of the experiment are to be published separately.

The writer wishes to take this opportunity to express his gratitude to Bruce Cork and William A. Wenzel for the privilege of joining with them in this experiment and for their generous advice in the publication of this paper.

The experiment was carried out under the auspices of the United States Atomic Energy Commission at the Radiation Laboratory of the University of California at Berkeley, California.

TABLE OF CONTENTS

LIST OF ILLUSTRATIONS AND TABLES

TABLE OF SYMBOLS AND ABBREVIATIONS

Bev	billion electron volts
c	velocity of light
c.m.	center of mass
d	length of target in direction of proton beam
$\frac{d\sigma'}{d\Omega'}$	differential cross section, center-of-mass system, for elastic proton-proton scattering
e	unit electron charge, 1.602×10^{-19} coulombs
E_1, E_2	relativistic energy of Particle 1 (outside proton)or Particle 2 (inside proton) in the laboratory system before collision
E_1^*, E_2^*	relativistic energy, laboratory system, of Particle 1 or 2 after scattering
E_1', E_2'	relativistic energy, center-of-mass system, of Particle 1 or 2 before collision
$E_1'^*, E_2'^*$	relativistic energy, center-of-mass system, of Particle 1 or 2 after collision
H	strength of magnetic field in gauss
K	monitor telescope calibration constant measured at each energy
kv	kilovolt = 1000 volts
ℓ	distance of travel of inside counter telescope along arc about the target
m_1, m_2	relativistic mass of Particle 1 or 2, laboratory system
m_1', m_2'	relativistic mass of Particle 1 or 2, center-of-mass system
m_{10}, m_{20}	rest mass of Particle 1 or Particle 2
mb	millibarn
Mev	million electron volts
msec	millisecond
N_m	number of monitor telescope counts
N_p	number of incident protons passing through a unit area of the target
N_{pp}	number of elastic proton-proton scattering events observed

N_t number of protons per unit volume in the target

p_1, p_2 momentum, laboratory system, of Particle 1 (outside proton), Particle 2 (inside proton) before collision

p_1^*, p_2^* momentum, laboratory system, of Particle 1 or 2 after collision

p_1', p_2' momentum, center-of-mass system, of Particle 1 or 2, before collision

$p_1'^*, p_2'^*$ momentum, center-of-mass system, of Particle 1 or 2, after scattering

R orbital radius of charged particle moving in a magnetic field

T_1^*, T_2^* kinetic energy of Particle 1 or 2, laboratory system, after collision

U total relativistic energy of both particles in the laboratory system

U' total relativistic energy of both particles in center-of-mass system

u velocity of the center of mass which is taken as the moving reference plane. (The center of mass is taken to move in the x direction).

v_1, v_2 velocity in laboratory system of Particle 1 or 2 before collision

v_{1x}, v_{1y} velocity in x, y direction, laboratory system, of Particle 1 etc., before collision

v_{1x}^*, v_{1y}^* velocity in x, y direction, laboratory system, of Particle 1, etc., after collision

v_1', v_2' velocity in center-of-mass system of Particle 1 or 2 before collision

v_{1x}', v_{1y}' velocity in x, y direction, center-of-mass system, of Particle 1, etc., before collision

$v_{1x}'^*, v_{1y}'^*$ velocity in x, y direction, center-of-mass system, of Particle 1, etc., after collision

β defined as $\frac{v}{c}$

thus: $\beta_c = \frac{u}{c}$,

$$\beta_{1x}^* = \frac{v_{1x}^*}{c},$$

$$\beta_{2y}' = \frac{v_{2y}'}{c}, \quad \text{etc.}$$

γ defined as $(1 - \beta^2)^{-1/2}$,

thus: $\gamma_c = (1 - \beta_c^2)^{-1/2}$,

$\gamma_{1y} = (1 - \beta_{1y}^2)^{-1/2}$, etc.

$\Delta\Omega'$ scattering solid angle, center-of-mass system, in steradians

θ_i angle of recoil, laboratory system, of proton scattered through the larger angle (inside proton, or Particle 2)

θ_1' angle of recoil, center-of-mass system, of the inside proton

θ_0 angle of recoil, laboratory system, of proton scattered through the smaller angle (the outside proton or Particle 1)

θ_0' angle of recoil, center-of-mass system, of outside proton

ω angular velocity in radians/sec

CHAPTER I

INTRODUCTION

Measurements of the differential cross section for elastic proton-proton scattering at energies of 100 to 345 Mev indicate that the cross section is practically independent of angle and energy in this range [1 - 7]. The angular distribution for elastic proton-proton scattering has also been reported for 437 Mev [8] and for 440 to 1000 Mev [9]. At these higher energies the elastic cross section becomes increasingly peaked in the forward direction--that is, at smaller angles in the center-of-mass system. Figure 1 is a plot of the cross sections reported for 440 to 1000 Mev [9].

Another consideration also requires that measurements be made at small laboratory angles. At low energies the angle in the laboratory system between the two recoiling protons from an elastic scattering event is 90°. At higher energies, where the recoiling protons possess relativistic velocities, this angle in the laboratory system is compressed kinematically. The relation of the angle (laboratory system) of scattering of the more energetic proton, θ_0, to θ_0', the center-of-mass scattering angle, is given by the relativistic equation

$$\tan \theta_0 = \tan \frac{\theta_0'}{2} \sqrt{\frac{2}{E+1}} , \qquad \text{(A -41)}^1$$

where E is the total energy of the incident proton in nuclear mass units.

At 6.2 Bev the angle between two particles recoiling at 90° in the center-of-mass system is 51.4° in the laboratory system. As another example, scattering at 10° (c.m.) at 6.2 Bev is observed with one counter at 2.4^{0} (lab).

---

[1] Scattering equations are developed in conveneint form in Appendix I. An equation number prefixed by an "A" denotes that this equation is taken from Appendix I.

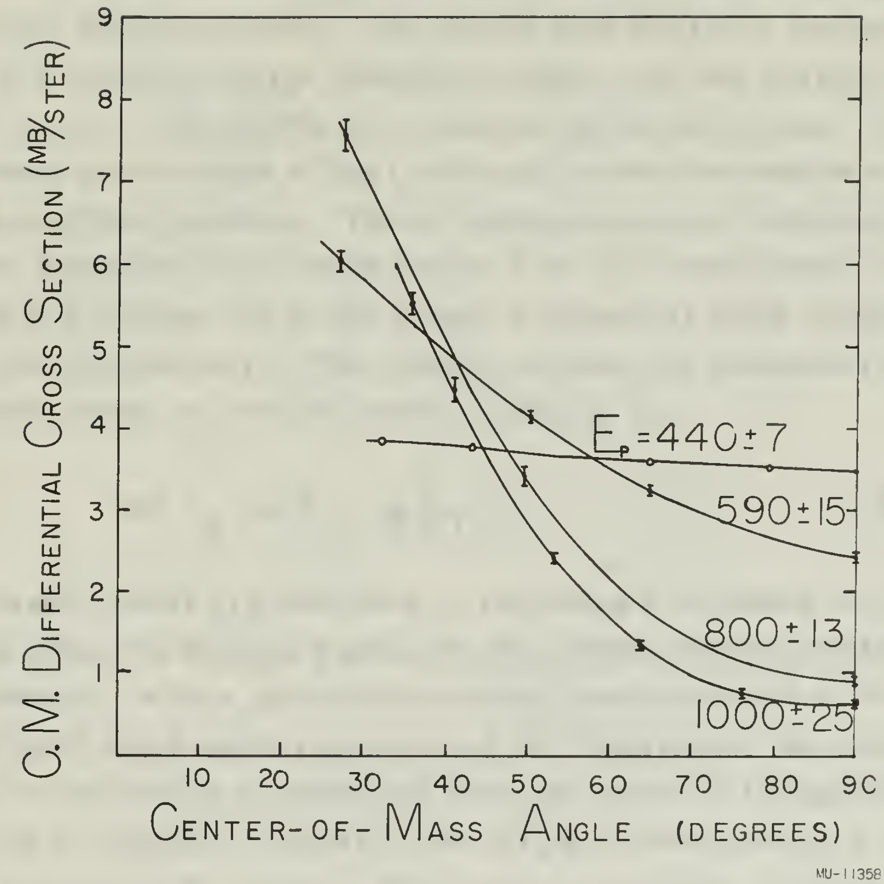

Fig. 1. Differential cross section of elastic proton-proton scattering in the center-of-mass system for proton energies of 440 to 1000 Mev measured at the cosmotron. [9]

Because of the inelastic reactions--such as π-meson, K-meson, and antinucleon production--that can occur at Bevatron energies, the scattered particles observed must fulfill criteria sufficient to ensure that the reaction observed is an elastic collision. Energetic protons of the Bevatron beam strike a polyethylene target in the upstream end of a Bevatron straight section. At small center-of-mass angles the more energetic proton, which is denoted the outside proton, is scattered at small angles in the laboratory system such that it is not deflected through the side of the straight section. The proton with the lower energy is scattered at a relatively large laboratory angle, and that scattered toward the center of the Bevatron is denoted the inside proton. The inside protons pass through a thin (.020-inch) aluminum window on the inside radius of the Bevatron. These inside protons are detected by a two-counter telescope; the outside proton from the same elastic event is detected by a counter set at the proper kinematical angle inside the Bevatron vacuum chamber. The relation between the laboratory angles of the outside proton θ_0 and the inside proton θ_i is

$$\tan \theta_0 \tan \theta_i = \frac{2}{E + 1} . \qquad \text{(A-46)}$$

The elastic events are observed by requiring a threefold coincidence between the properly delayed signals of the outside counter and the inside telescope. With a coincidence circuit resolution of 6×10^{-9} second and good solid-angle resolution of 10^{-4} steradian, the elastic-scattering cross section is separated from the inelastic background.

The flux of energetic protons at the target is measured by a monitor telescope directed at the target. The monitor telescope counting rate is calibrated against the number of beam protons as measured by an electrostatic induction electrode in another Bevatron straight section. Figure 2 illustrates the arrangement of counters and target used.

In this cross-section measurement with the internal beam of the Bevatron, the physical structure and the operating characteristics of the accelerator placed certain limitations and demands on the equipment used.

[illegible]

[illegible]

[illegible]

[illegible]

[illegible]

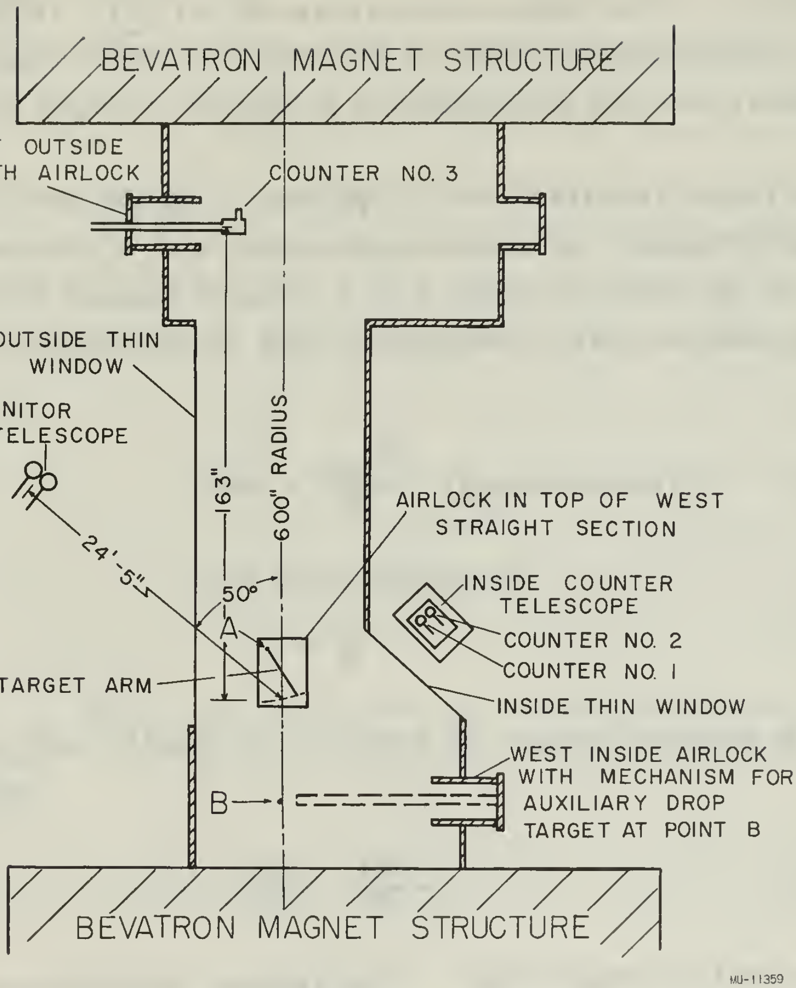

Fig. 2. Bevatron west straight section schematic with positions of the targets and counters used in the proton-proton scattering experiment indicated.

CHAPTER II

CHARACTERISTICS OF THE BEVATRON PROTON BEAM

The Bevatron is a proton synchrotron accelerator which employs the principle of phase stability independently suggested by Veckslar [10] and McMillan [11] for the acceleration of particles to relativistic velocities. Phase-stable particles can be made to undergo slow, small changes in their angular velocity or orbital radius and still remain phase stable.

A particle with charge e, energy E, and relativistic mass m, moving with velocity v in a plane perpendicular to a magnetic field H, will move with an angular velocity ω in a circle of radius R, in such a way that the inductive force Hev is balanced by the centrifugal force mv^2/R:

$$Hev = \frac{mv^2}{R} \quad \text{(gaussian units)}; \tag{1}$$

ω can be expressed as

$$\omega = \frac{v}{R} . \tag{2}$$

Combining Eqs. (1) and (2), we have the angular velocity of the particle given by

$$\omega = \frac{He}{m} = \frac{Hec^2}{E} , \tag{3}$$

where E is the relativistic energy mc^2. The frequency of the accelerating electrostatic field is usually matched to this ω. Equations (1) and (3), combined with the principle of phase stability, suggest several methods for the acceleration of particles to relativistic energies.

In the synchrocyclotron, the stable orbits of the particles in a uniform magnetic field are periodically increased by a periodic variation of the cyclotron oscillator frequency. As the maximum energy of the

accelerator increases toward 1000 Mev, the proton orbital radius demands such a large-core magnet that a slightly more complicated accelerating technique becomes more practicable.

In the proton synchrotron, protons are accelerated in a more or less fixed orbit by variation of both the magnetic field and the frequency of the accelerating electric field.

In the Bevatron the particle travels in an orbital magnetic field whose strength increases as energy is supplied in small increments to the particle. Protons are periodically injected into the Bevatron at an energy and radius appropriate to the initial magnetic field and accelerating frequency. After injection, H and ω are increased until the proton reaches the desired energy. Beam-focusing forces are supplied by spatial variation of the magnetic field strength, i.e., betatron focusing.

The Bevatron consists of a large annular magnet, divided into quadrants, with 20-foot straight sections between quadrants which provide field-free space for the proton injector, accelerating electrode, vacuum pumps, monitoring electrode, targets, etc. A Cockcroft-Walton accelerator begins the proton acceleration, sending 450-kev protons to a linear accelerator which feeds the protons into the Bevatron field after acceleration to 9.9 Mev.

Figure 3 is a diagram of the Bevatron, showing dimensions and relative locations of the various components. Table I lists Bevatron characteristics.

The value of final energy reached is chosen by turning off the accelerating (rf) voltage. Here it is convenient to rewrite Eq. (3) as

$$E = \frac{Hec^2}{\omega} \quad . \tag{4}$$

After rf turnoff, H continues to increase, causing the equilibrium orbit to shrink. Energetic protons are thus "spilled" onto a target placed at a smaller radius. The turnoff of the rf field is actually triggered when the magnet current reaches a preselected value. The energy of the particles at spill-out is known to within ±1%. The error in the

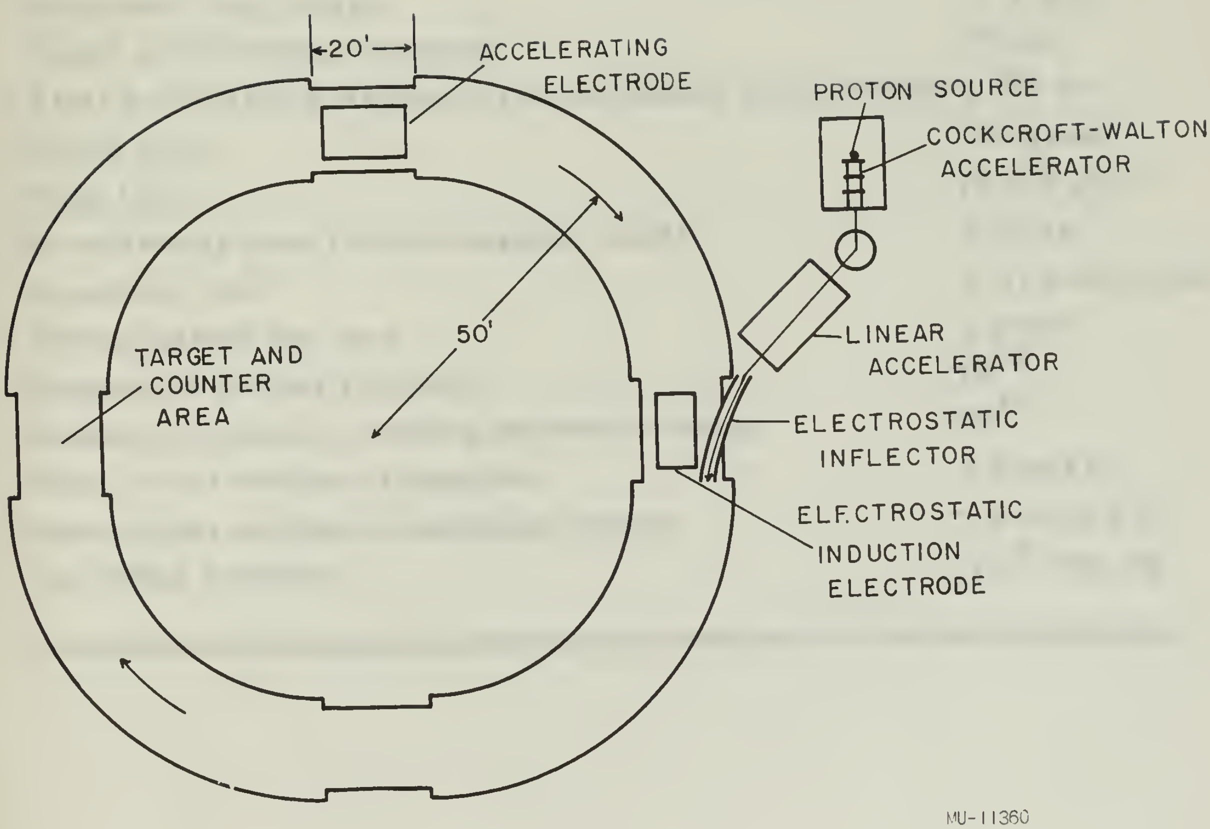

Fig. 3. Bevatron schematic.

Table I

Bevatron Characteristics	
Radius of equilibrium orbit	600 in.
Length of straight sections	20 ft
Injection energy	9.9 Mev
Maximum final energy	6.3 Bev
Initial accelerating frequency	356 kc
Final accelerating frequency (for maximum acceleration)	~2, 500 kc
Initial field	~300 gauss
Peak field	~15,870 gauss
Accelerating time (rising magnetic field)	1.75 sec
Repetition rate	6-17 pulses/min
Energy gained per turn	1.5 kev
Number of protons injected	$\sim 10^{13}$
Number of protons reaching maximum energy	$\sim 10^{10}$
Beam cross section at injection	1 ft by 4 ft
Beam cross section at maximum energy	~1.5 in. by 4 in.
Operating pressure	$\leq 10^{-5}$ mm Hg

average H at cutoff is known to less than ±0.3%. Additional error is due to deviation of the beam center from the nominal path and to shift in the current markers ("I pips") with respect to the magnet current. Error due to betatron and phase oscillations is negligible [12] .

The beam can be spilled out more slowly, but with a spread of energy over the time of slow spill-out of ~4 Mev/msec. This slow spill-out is achieved by reducing the magnitude of the accelerating voltage at the time slow spill-out is to begin. The voltage applied to the accelerating electrode is reduced from 20 kv to 10 kv. At this time protons that are just barely phase stable will not receive enough energy to keep up with the increasing field and will spiral inward to the target. A second method of achieving this slow spill-out is to apply 1 kc noise modulation to the accelerating rf at the time the voltage is reduced.

CHAPTER III

EXPERIMENTAL EQUIPMENT

1. Targets and Target Mechanisms.

The proton beam of the Bevatron is as yet an internal beam. Targets for the energetic protons were placed within the beam aperture at a position that would allow both protons scattered from the elastic collision to be observed. Figure 2 is a schematic diagram of the west straight section, which has been fitted with sundry air locks allowing target mechanisms and counter mechanisms to be placed or plunged as appropriate.

For measurement of scattering at angles of 10° (lab) and less, our polyethylene (CH_2) target was suspended from the arm of a probe inserted in an air lock in the top of the straight section. The probe was centered at point A, as indicated on the diagram (Fig. 2), and was free to turn so that the arm of the probe shaft could move in the horizontal plane. In this manner the target could be moved in an arc, as shown, over a range of Bevatron radii from 592 to 607 inches. The proton beam could be tracked and spilled onto the target at radii of 596 to 604.5 inches. With this freedom of movement of the target, protons scattered through an angle of 10° (lab) could be picked up by a counter placed inside the straight section. The complementary protons from these elastic events could be detected by the counter telescope through the thin (0.020-inch) inside window. With the target in this position the inside telescope could view protons scattered from 50° to 95° (lab). The horizontal dimension of the solid angle is defined by the width of the scintillator of counter No. 3. Good angular resolution is achieved by placing this counter as far from the target as is consistent with a reasonable counting rate from the counter. The position of this counter when placed inside the straight section is limited by the Bevatron field at the end of the straight section. Location of the target along the arc about point A, then, fulfills the requirement of greatest distance between target and counter while yet

CHAPTER III

EXPERIMENTAL EQUIPMENT

1. Targets and Target Mounting

[illegible]

[illegible]

permitting the target to be viewed at angles up to 90° by the inside telescope.

To measure the scattering at larger center-of-mass angles, the target was suspended at point B from an arm inserted into the straight section through an air lock on the inner side. Counters on the outside could view protons from this target through a thin window on the outside of the straight section at laboratory angles from 10° to 40°, while the complementary proton could be viewed at angles from 30° to 65°.

At injection the proton beam fills the Bevatron aperture; as acceleration progresses, the beam contracts to a cross section of about 1.5 by 4 inches. Any object in the aperture at injection or during the early acceleration effectively scatters all the beam before any appreciable acceleration can occur. Targets for the internal beam are arranged to be retracted out of the aperture at injection and are raised or dropped into a position level with the median plane of the beam just prior to start of beam spill-out at desired energy. Our target probe was fitted with a small rotary solenoid which, when triggered, would drop the target on a pair of threads tied to a movable arm. Figures 4 and 5 show the bottom of the target mechanism probe with the small polyethylene target in the up and extended positions.

As the scattering angle (c.m.) becomes smaller, the inside proton (i.e., the proton scattered through the larger angle) possesses less energy. In order for all elastic-scattering events to be observed, protons from the outside of the target scattered toward the inside telescope must possess sufficient energy to pass through the target, through a 0.020-inch aluminum window, and through the scintillator of the first counter of the telescope, and yet possess sufficient energy upon reaching the second counter to be detectable. In addition, it is desirable for the time of flight for a proton leaving the outside of the target to be within 10^{-9} second of a proton leaving the inside of the target, in order to maintain good time resolution against inelastic particles. For the measurement of the elastic cross section at angles where the outside laboratory angle was 8° or less, the polyethylene target was made only

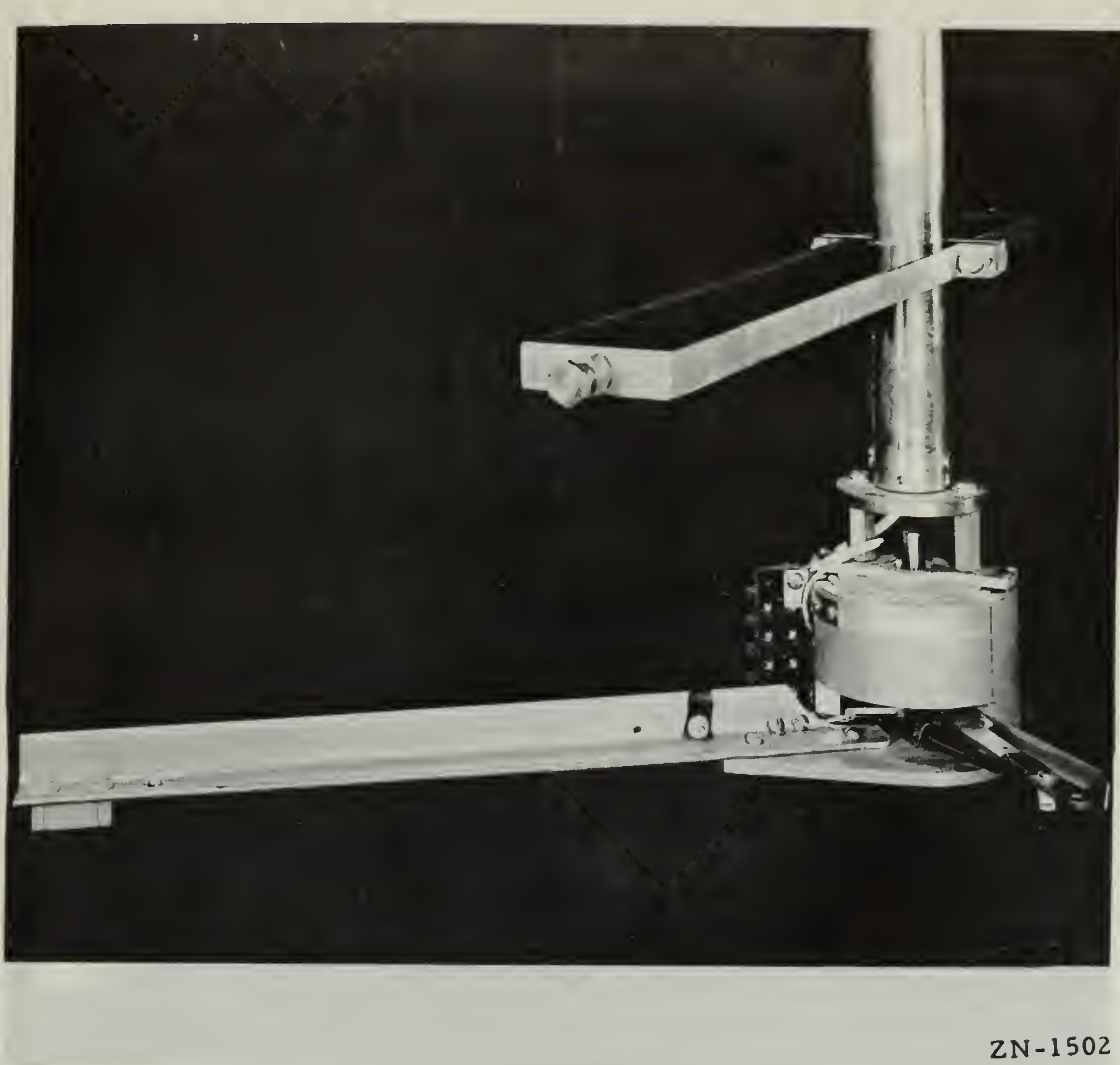

Fig. 4. Target probe with dropping mechanism and target. Rotary solanoid for dropping target is contained in cylindrical housing at bottom of probe at right. Polyethylene target 1/16 by 0.5 by 1.5 inches is pulled up in retracted position under the left end of the fixed arm.

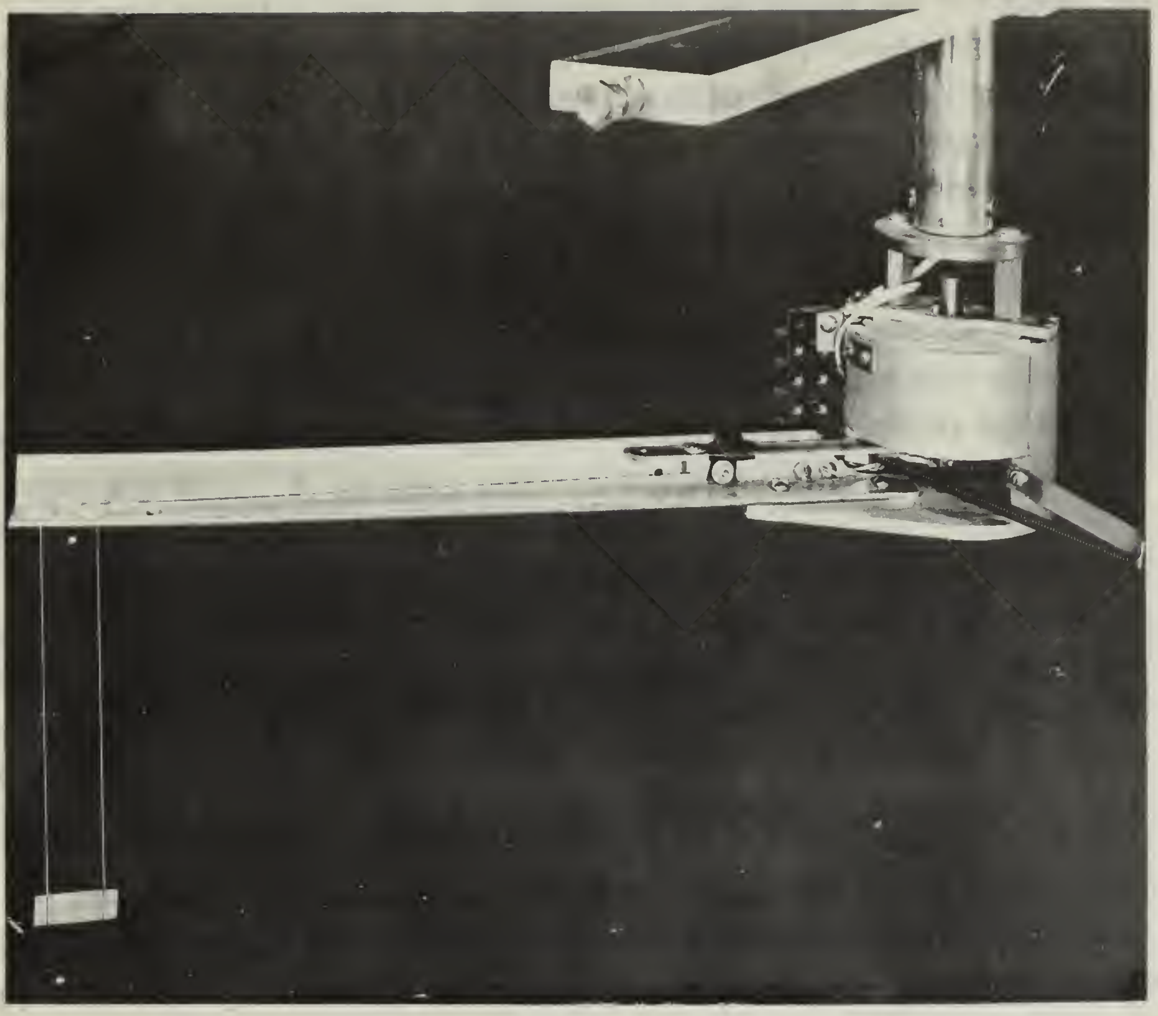

ZN-1503

Fig. 5. Target probe and target. Target suspended by two nylon threads is in the down position in lower left corner.

1/16 inch thick. A proton of 30 Mev lost only ~ 4 Mev in traversing the breadth of this target. The difference in times of flight of protons from inside and outside edges of the target amounted to only 0.9×10^{-9} sec for 2° outside laboratory angle at 6.2 Bev.

A good practical vertical dimension for the target was 0.5 inch. A greater height would have required that the vertical dimension of the No. 2 counter scintillator be increased to encompass all the scattering events observed by the No. 1 counter. The length of the target was then made 1.5 inches so as to place sufficient mass at the target to ensure that enough elastic scattering events occurred per Bevatron pulse to be observable above background noise.

At angles where θ_0 exceeds 8°, the kinetic energy of the inside proton exceeds 100 Mev for bombarding energies of 2.24 Bev and over. Therefore, at angles where θ_0 exceeded 8°, a target 1/8 by 0.5 by 1.5 inches was used. A 100-Mev proton loses less than 2 Mev energy in passing through this 1/8-inch polyethylene.

The heavier target was dropped easily enough on strings of substantial strength. The 1/16-inch target, though, showed a tendency to sway and bounce when lowered on light fishing line. The light target was eventually suspended by nylon sewing thread, size "A", with which it dropped smoothly.

2. Scattering Event Counters and Electronics.

The counters used to detect the scattered protons were terphenyl-loaded polystyrene scintillators viewed through short lucite light pipes by RCA 1P21 photomultiplier tubes. The signals were developed across 120-ohm resistors at the multiplier anodes, and were transmitted through about 200 feet of 125-ohm coaxial cable to 200-ohm delay boxes, where time delays were matched and where the proper time-of-flight difference for the inside and outside protons could be set. To prevent signal reflections the impedance of the 125-ohm cable was matched to the 200-ohm delay boxes by teeing a 330-ohm resistor in parallel with the 200-ohm input. The impedance of all electronic equipment from

[illegible]

[illegible]

[illegible]

[illegible]

[illegible]

[illegible]

[illegible]

the delay boxes through the pulse shaper was 200 ohms, and impedance mismatches were not a problem. The output of the pulse shaper was matched to the decade scalers.

A block diagram of the electronic equipment used is shown in Fig. 6. After passing through the delay boxes, the signals were passed through a Hewlett-Packard 460 A wide-band amplifier. Each signal was then split and passed through another Hewlett-Packard 460 A. At this point two separate signal channels, A and B, were possible, each channel with an input signal from the three counters used to observe the scattering. The signals were fed into a two-channel threefold coincidence circuit. The coincidence circuit was a pentode plate addition type. The plate pulses were clipped to a duration of 4×10^{-9} second by shorted 2-foot cables at the pentode plates. The resolving time of each coincidence channel was about 6×10^{-9} second. The resolving time is the measured time spread of input signals which give an output coincidence signal of one-half the maximum output of the threefold coincidence. The output coincidence pulses of each channel were amplified by two Hewlett-Packard 460 A's and fed to pulse shapers whose output was a 10-volt 0.1-microsecond pulse suitable to drive the Hewlett-Packard 520A High-Speed Decade Scalers. The pulse-shaper circuits had a discriminator input which permitted rejection of the small twofold coincidence output in the threefold coincidence circuit. The decade scalers were backed up by UCRL fast scale-of-1000 scalers.

The No. 3 counter, which observed the outside proton, was used to define the horizontal dimension of the scattering solid angle, since the outside proton was the more energetic and would suffer the less scattering en route to its counter. The scintillator of this counter was 2 by 0.5 by 0.25 inch. Scintillator and photomultiplier tube were placed inside an airtight head mounted on a probe shaft and extended into the Bevatron straight section through an air lock on the outside forward end of the west straight section. The probe passed into the air lock through a chevron seal so that the distance the counter reached into the straight section was readily adjustable. At this point the counter was

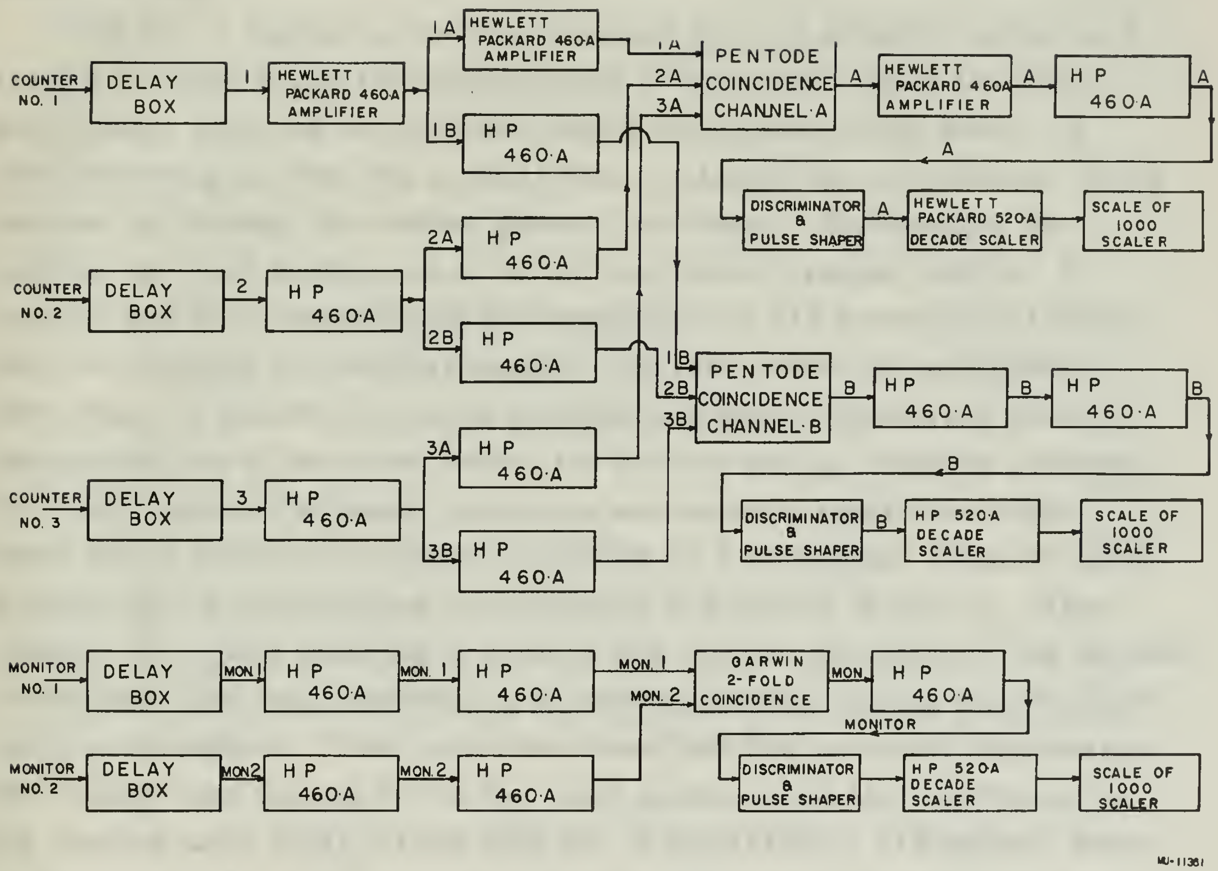

Fig. 6. Block diagram of electronics equipment and scalers used with the scattering counters and the monitor telescope.

in a magnetic field that attained ~1700 gauss at maximum energy. The No. 3 counter could not have been located farther along the straight section without encountering magnetic field of serious magnitude. The photomultiplier tube was well shielded with a steel sheath and a mu metal liner. When this counter was assembled its efficiency was tested with a radium γ-ray source in a calibrated magnetic field. The efficiency of the No. 3 counter for γ-rays versus external magnetic field is shown in Fig. 7.

The No. 3 counter probe was inserted into the straight section at a level 5.5 inches below the median plane of the beam. Here the probe and counter head did not interfere with acceleration of the beam. A tube extending up from the counter head contained the scintillator, which reached up through the median plane of the beam. To measure the scattering cross sections at 4° in the laboratory system, the No. 3 counter had to be located with its scintillator at 615 inches (and further into the aperture for smaller angles). At this radius the scintillator tube began to interfere with the accelerating beam, scattering most of the protons out of the beam before the desired energy could be achieved. To avoid this loss of beam, provision was made to rotate the probe shaft with a small air cylinder controlled by a Modernair solenoid valve. Counter No. 3 with rotating arrangement is pictured in Fig. 8. When counter No. 3 was inserted to radii of 615 inches and smaller, the counter scintillator tube was rotated to a horizontal position during injection and early acceleration. Then, after the beam had contracted at high energy, the counter was flipped 90° to the erect position with the scintillator at the median plane level. Even with No. 3 counter in to 610 inches, beam of the magnitude of 10^{9} protons per pulse was possible when the counter was rotated in this manner. Most of the cross-section measurements were made at beam intensity of the order of 2×10^{8} protons per pulse.

As previously mentioned, one of the major limitations of the measurement of cross sections into very small angles is the rapid fall-off of energy of the inside proton. To allow the passage of protons of 30 to 40 Mev from the target into the second counter of the inside telescope, the scintillator of the first telescope counter, the No. 1 counter,

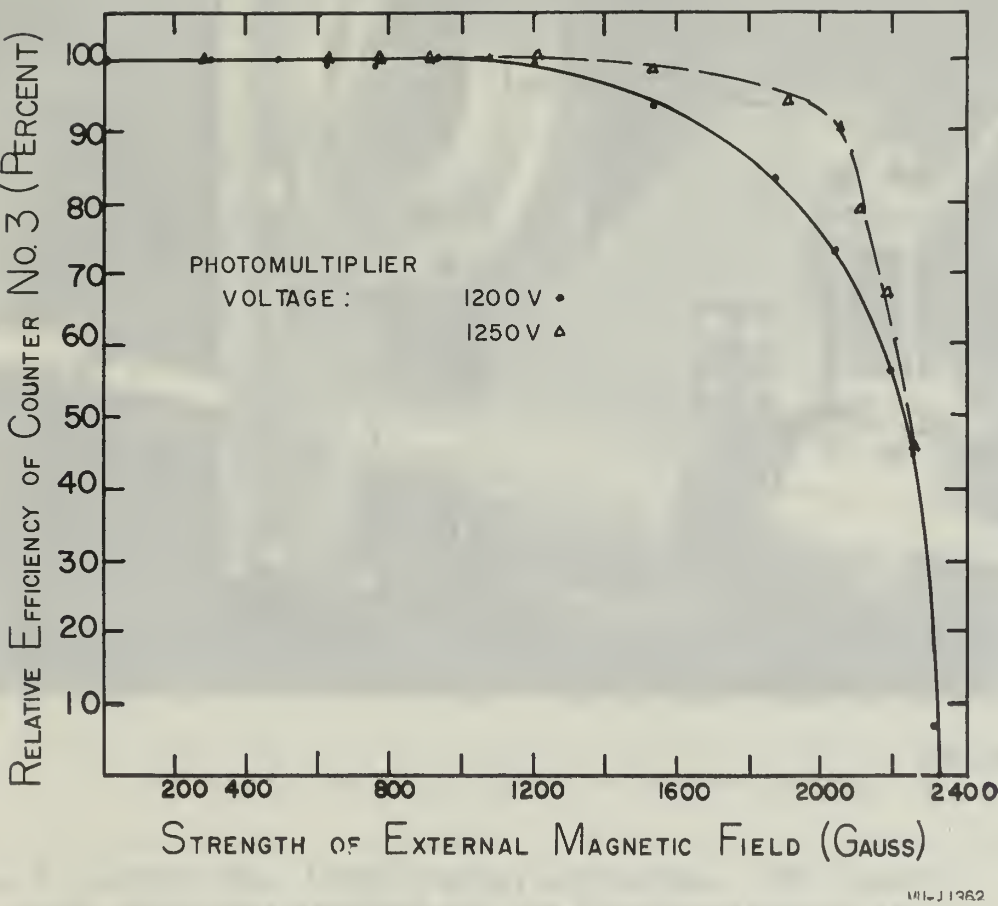

Fig. 7. Counting efficiency of counter No. 3 in magnetic field.

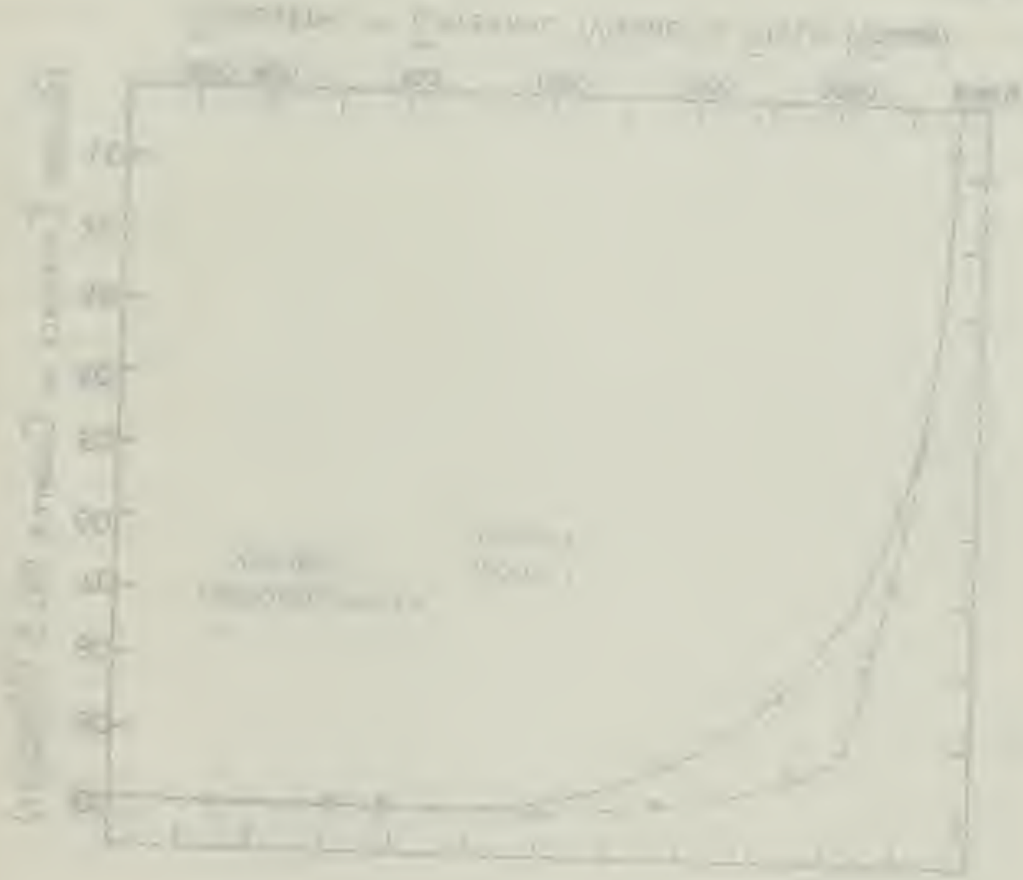

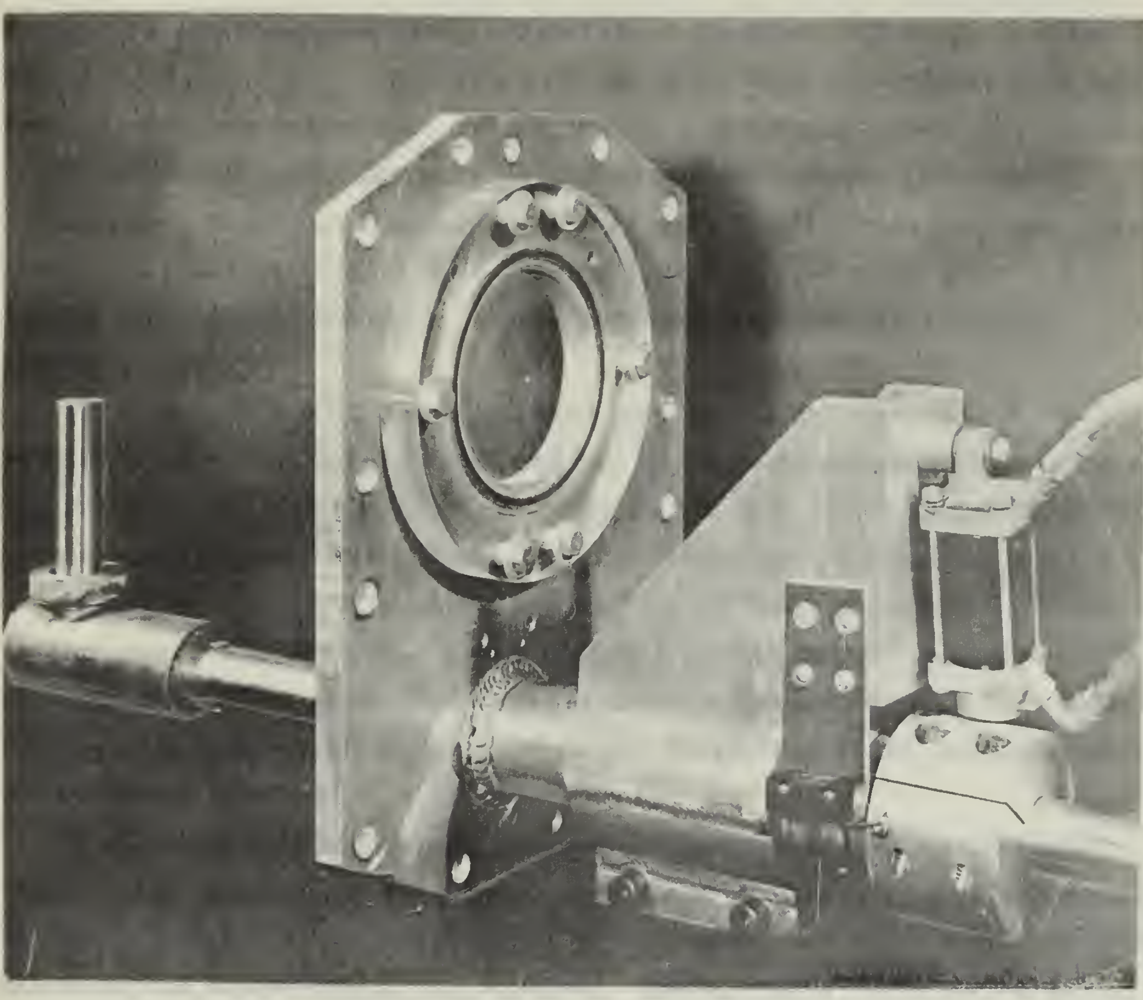

ZN-1500

Fig. 8. Counter No. 3 with rotating mechanism. The counter bend, which was extended into the Bevatron vacuum, is at left. The shielded photomultplier tube is contained in the enlarged cylinder at the end of the probe; the scintillator is within the vertical tube at left. The small air cylinder used to rotate the probe is at right.

was made only 1/16 inch thick for the measurement of cross sections below 8^{o} outside angle (lab). It was important to enclose this scintillator in the thinnest practicable lighttight material. An effective lighttight enclosure was made by using a 0.001-inch duralloy foil on each side. The efficiency of No. 1 counter with the 1/16-inch scintillator was tested in a cosmic-ray telescope. The efficiency remained effectively 100%.

With the thin (0.020-inch) Bevatron window and the 1/16-inch scintillator, a proton leaving the target with 30 Mev energy would reach the No. 2 counter with 17 Mev remaining. A proton of 20 Mev at the target would have, perhaps, 1 Mev remaining on reaching counter No. 2.

The scintillator of No. 1 counter was 1 inch by 1 inch in cross section. The 1-inch height defined the vertical dimension of the scattering solid angle. (The method of covering the 1.5-inch horizontal dimension of the target with the 1-by-1-inch scintillator is taken up later.)

Counter No. 2 had a scintillator of rough circular shape 2.75 inches in diameter. Counter No. 2 was placed 5 inches behind counter No. 1 and effectively covered all the target area projected through No. 1; its area was large enough to encompass the scattering of the inside proton in the No. 1 counter.

The inside telescope was mounted so that the counter scintillators were in the same plane as counter No. 3 and the target. The telescope was located as near as practicable to the inside thin window to minimize the effect of scattering in the window. The distance from the target to the first telescope counter varied from 60 inches to 72 inches. Scattering in the thin window was always negligible. At this distance the counters at times operated in magnetic fields of ~20 to 30 gauss. The counters were well shielded against fields of this magnitude.

3. Monitor Telescope Counters and Electronics.

The monitor telescope consisted of two RCA 6199 photomultiplier tubes viewing terphenyl-loaded polystyrene scintillators. The monitor telescope, directed toward the target position, was placed 24 feet 5

inches from the target at an angle of 50° on the outside of the target. The signals were developed across a 120-ohm resistor in the photomultiplier anode and transmitted through about 200 feet of matched 125-ohm cable to two Hewlett-Packard 460A wide-band amplifiers. The 125-ohm cable was matched to the 200-ohm input of the Hewlett-Packard amplifiers by placing 330 ohms in parallel with the amplifier input. The amplified signals were fed to a two-channel Garwin-type pentode coincidence circuit. The coincidence signal was amplified by a Hewlett-Packard 460A amplifier, sent through a pulse shaper, as with the scattering coincidence signals, and fed to a Hewlett-Packard 520A High-Speed Decade Scaler backed up with a UCRL fast scale-of-1000 scaler.

All scalers , both in monitor and scattering channels, were gated to count for only 100 milliseconds after the start of beam spill-out.

CHAPTER IV

EXPERIMENTAL PROCEDURE

1. Calibration of the Monitor Telescope.

The number of proton-proton elastic scattering events N_{pp} observed in the center-of-mass solid angle $\Delta\Omega'$ is

$$N_{pp} = \Delta\Omega' \frac{d\sigma'}{d\Omega'} N_p N_t d, \tag{5}$$

where $\frac{d\sigma'}{d\Omega'}$ is the differential cross section (c.m.) for proton-proton elastic scattering,

N_p is the number of bombarding protons passing through a unit area of the target,

N_t is the number of protons per unit volume in the target, and

d is the length of the target in direction of the proton beam.

Then we have

$$\frac{d\sigma'}{d\Omega'} = \frac{N_{pp}}{\Delta\Omega' N_p N_t d} . \tag{6}$$

It is convenient to calibrate the monitor telescope directly in terms of $N_p N_t d$; the counting rate of the monitor at a given energy depends on the number of protons passing through a unit area of the target N_p and the number of protons behind a unit area of the target $N_t d$.

To calibrate the monitor, the small target was replaced with a polyethylene target 1 by 1 by 3 inches with a 0.5-inch lip 0.25 inch thick. This target is illustrated in Fig. 9. The lip extends radially outward from the forward edge of the target. In effect, the target lip expedites the spilling of the beam into a thick target. Protons passing through the lip lose enough energy to reduce their radius for the succeeding turn from the normal 1/3 mil to ~ 1/8 to 1/4 inch, so that the majority of the protons pass directly through the full target thickness after one

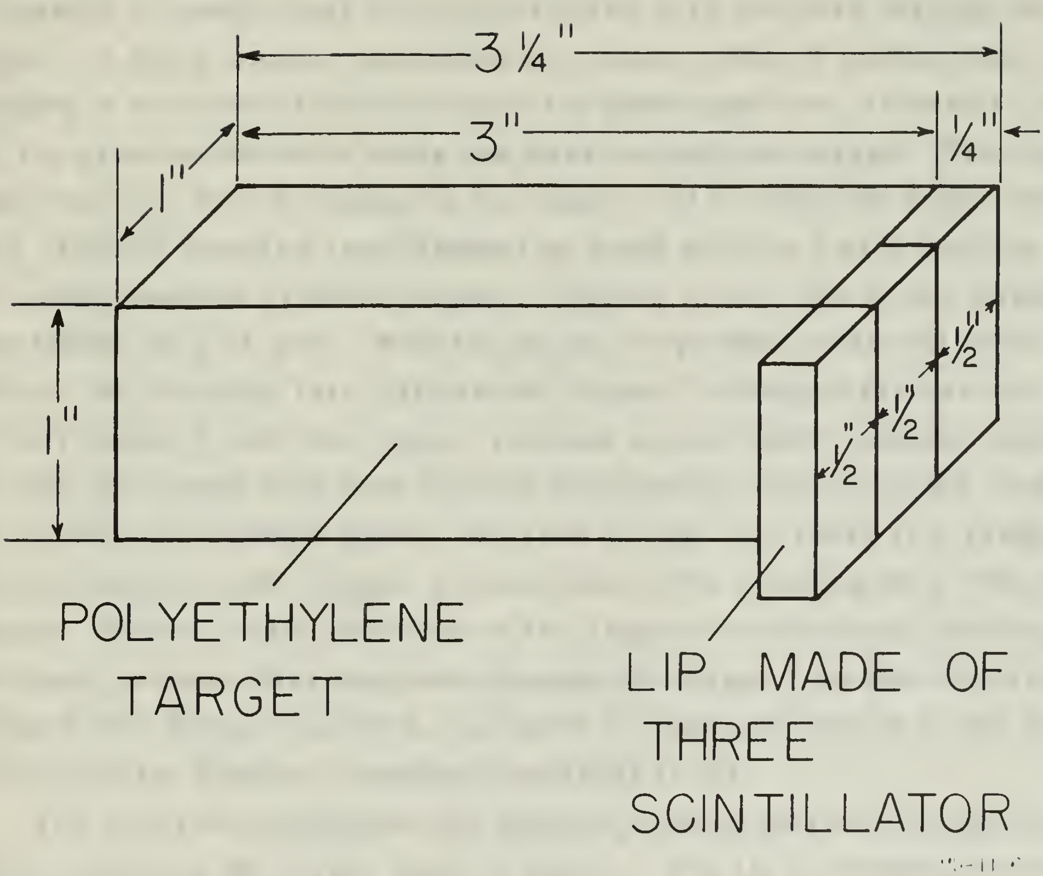

Fig. 9. 1 x 1 x 3 inch polyethylene target with lip.

or two passes through the lip and are not scattered away by a grazing encounter with the target, as might occur if the beam were to spiral into the target at the normal 0.0003 inch per turn [12]. The theory of the lip target has been published by McMillan [13].

The counting rate of the monitor is then calibrated against the number of protons per pulse in the beam as measured by an electrostatic induction electrode. It is assumed that effectively all of the protons in the beam will pass through the 1-by-1-by-3-inch target. In this calibration it is necessary to ensure that the protons make only one pass through the target. A beam clipper consisting of a copper plate 4 inches thick, plunged in an outward direction into the beam aperture, is used to scatter the protons that have made one pass through the target. The clipper experiment is done by plunging the clipper out to different radii, measuring [Monitor counting rate/Number of beam protons] as a function of the radial position of beam clipper. Figure 10 is a plot of the clipper experiment at 2.24 Bev. With the target suspended at the 604-inch radius, the counting rate falls as the clipper is plunged farther and farther outward until the clipper reaches a point where protons passing through the target pass next through the clipper, are scattered, and do not return to the target again. As seen in Fig. 10, there is a range of several inches in the clipper position where the counting rate remains steady. This is at the point where the clipper is effectively blocking all the beam protons after one pass through the target. As the clipper is plunged still farther outward, the beam is scattered before it can strike the lip and the monitor counting rate drops to nil.

For accurate calibration the number of beam passes through the lip before reaching the target must be known. The lip is constructed of three 0.5-inch terphenyl-loaded polystyrene scintillators (refer to Fig. 9). By measurement the relative C^{11} beta activity induced in each of the three scintillators after exposure to the beam, the ratio of lip passages to target passages is obtained. At the energies this experiment is concerned with, this ratio is roughly 2 to 1. The effective target distance traversed by the beam making two passes through the 1/4-inch-

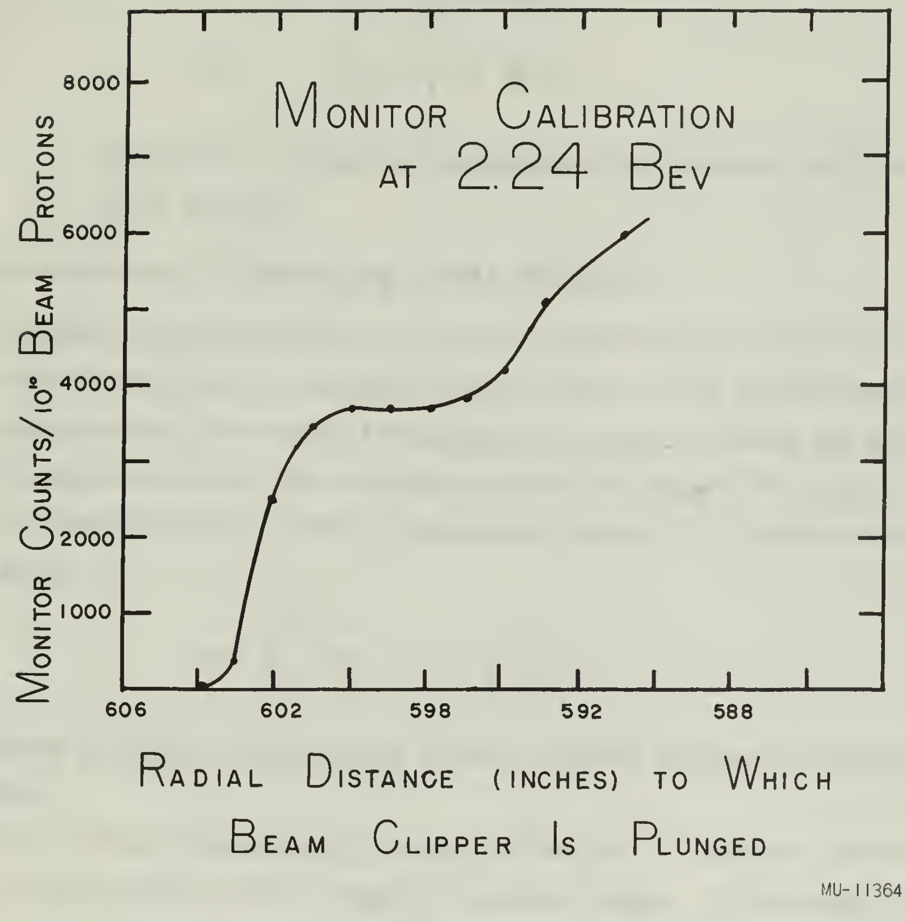

Fig. 10. Plot of data taken to calibrate monitor telescope against the induction electrode at 2.24 Bev. There is a plateau in the counting rate for clipper positions at 597 to 600 inches where beam protons make only one traversal of the target.

thick lip and one pass through 1/14 inch of scintillator and 3 inches of target is then 3.75 inches. The ratio

$$\frac{\text{Monitor Counts}}{\text{Number of Beam Protons/Unit Area x Hydrogen Nuclei in Target/Unit Area}}$$

$$= \frac{N_m}{N_p N_t d}$$

is then obtained. This can be rewritten

$$N_m = (N_p N_t d) \times K, \tag{7}$$

where K is a number measured for monitor calibration at each energy.

2. Measurement of Scattering Cross Sections.

To measure the number of protons elastically scattered through the solid angle subtended by outside counter No. 3 at a given energy and laboratory angle, the inside telescope is centered along the kinematically correct angle to detect the complementary proton of the elastic event. The relationship of the outside laboratory angle θ_0 to the inside laboratory angle is

$$\tan \theta_0 \tan \theta_i = \frac{2}{E + 1}, \tag{A-46}$$

where E is the total energy of the incident proton in nuclear mass units.

The vertical dimension (1 inch) of the No. 1 counter defines the vertical dimensions of the scattering solid angle. The target is 1.5 inches long; in this experiment the scintillator of No. 1 counter was held to 1 inch in the horizontal direction to keep down the number of particles, elastic and inelastic, that this counter would have to view at any time. The No. 3 counter sees an end-on view of the target. In order to span the area where the inside protons could be scattered from the target in elastic events observed by counter No. 3, it was necessary

[illegible]

[illegible]

$$[illegible]$$

[illegible]

$$[illegible]$$

[illegible]

[illegible]

[illegible]

$$[illegible]$$

[illegible]

[illegible]

to move the inside telescope in an arc around the target to either side of the inside angle θ_i. Figure 11 is a photograph of the selsyn-driven cart used to carry the inside counter telescope along its required arc. If the number of scattering events observed at any position along the arc swept by the inside telescope is plotted as a function of position along the arc, the total number of events observed for a given outside laboratory angle is then the integral along the arc of events observed at each position on the arc:

$$N_{pp} = \int_{-\infty}^{\infty} n(\ell)\, d\ell, \tag{8}$$

where $n(\ell)$ is the number of events per 1000 monitor counts per unit distance along the arc, and ℓ is distance in inches along the arc.

Figure 12 is a typical plot of the counting rate as a function of inside telescope position on the arc.

The outside counter was located at ~ 163 inches from the target, the inside telescope at 60 to 72 inches from the target. The signals from the telescope and the No. 3 counter were properly delayed with respect to each other to allow for the different times of flight for the two elastically scattered protons. The velocities of the protons observed at various laboratory angles are obtained from the equations

$$\tan \frac{\theta_0'}{2} = \sqrt{\frac{E+1}{2}} \tan \theta_0, \tag{A-41}$$

$$E_{1,2}^* = \frac{E+1}{2} \left(1 - \frac{E-1}{E+1} \cos \theta_0'\right), \tag{A-52}$$

$$\beta_{1,2}^* = \frac{\sqrt{E_{1,2}^{*2} - 1}}{E_{1,2}^*}, \tag{A-55}$$

where E is in units of nuclear rest mass.

[illegible]

$$[illegible]$$

[illegible]

[illegible]

[illegible]

$$[illegible]$$

$$[illegible]$$

$$[illegible]$$

[illegible]

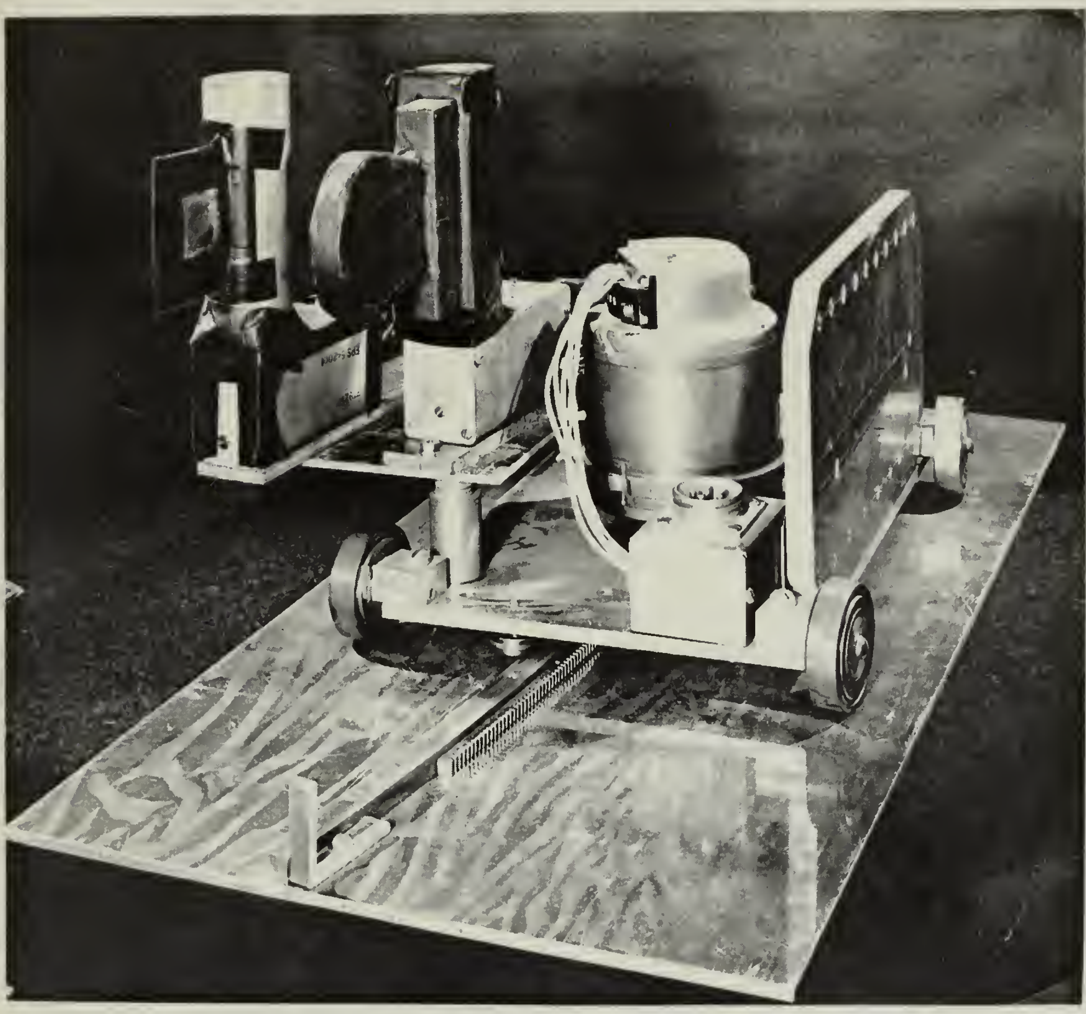

ZN-1501

Fig. 11. Inside counter telescope on remotely controlled cart. Counter No. 1 with 1-by-1-by-1/16-inch scintillator is at left. Counter No. 2 is at left center. The selsyn motor used to drive cart along the curved rack is at center of cart.

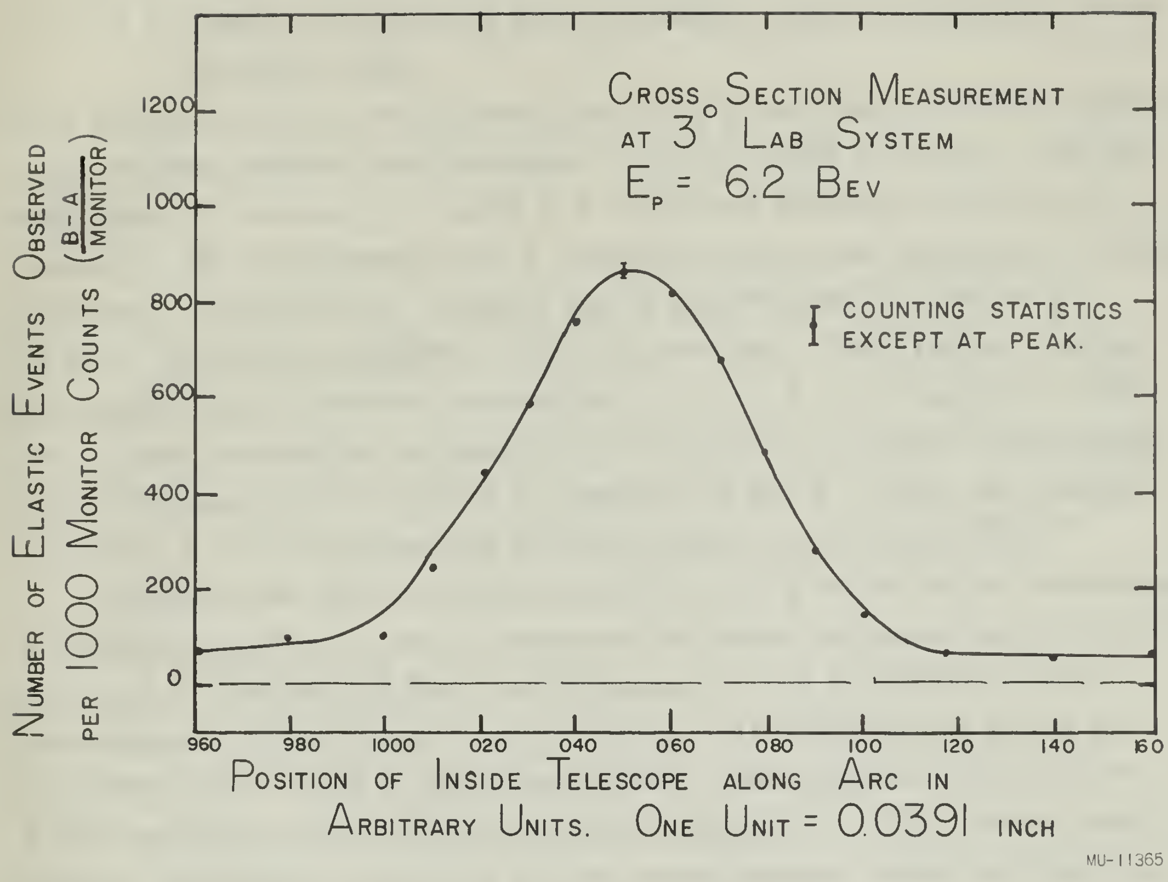

Fig. 12. Accidental events have been deducted before plotting. The background extending to either side of the peak is due to proton-carbon events. Elastics events are then the integral under the curve minus the area due to this background. Errors indicated are counting errors only.

The coincidence signals of the properly delayed counters set at the proper angles are then produced by

(a) elastic proton-proton scattering,

(b) proton scattering from carbon in the target,

(c) accidental background due to multiply scattered particles from inelastic events.

It is assumed that the background level at a given energy is at a constant level for any counter delay settings. As previously described, the signals from the counters are split and fed to two separate coincidence channels. In one channel--the B channel--the proper kinematical delays were set. In channel A, counter No. 3 was delayed an arbitrary 15×10^{-9} second in addition to the proper delay. The arbitrary delay was applied in a direction to avoid the $p + p \rightarrow d + \pi^{+}$ reaction. Channel A then counted the accidental events from the inelastic background. The difference between counts in Channels B and A is then the number of elastic p-p events plus any proton-carbon scattering present.

To determine the correction necessary for proton-carbon scattering, a graphite target was used to measure the extent of proton-carbon scattering at 5° (lab) at 6.2 Bev, with Channels A and B delayed as for measurement of proton-proton scattering. At this angle no peaks were observed in the curve of the counting rate plotted against the position of the inside telescope. The only effect noted was a level steady background, which was present on all the proton-proton scattering counting-rate curves.

The number of elastic scattering events observed at the particular laboratory angle was then the integral of the area under the [Channel B minus Channel A] counting-rate curve after the level background due to proton-carbon scattering was subtracted (refer to Fig. 12).

The differential proton-proton elastic scattering cross section is then known; combining Eqs. (6), (7), and (8), we have

$$\frac{d\sigma'}{d\Omega'} = \frac{N_{pp}}{\Delta\Omega' N_p N_t d} = \frac{KN_{pp}}{\Delta\Omega' N_m} = \frac{K \int_{-\infty}^{\infty} n(\ell)\, d\ell}{\Delta\Omega' N_m} . \quad (9)$$

To measure the scattering cross section at large angles (center of mass), where the outside counter must be located outside the Bevatron straight section, the No. 3 counter is replaced by a two-counter telescope directed at the target. The addition of this telescope reduces the background level and permits the measurement of the cross section, which is relatively small at these angles. The cross section is so large, in general, at small angles (center of mass) at Bevatron energies that there is no difficulty in separating the elastic-scattering peak from the inelastic background by using only the single counter to detect the outside proton.

To check that the counters were operating with sufficiently high voltage for the photomultipliers, and that the large magnetic field did not cause the counting rate of counter No. 3 for protons to fall off, the high voltage was varied over a range from 1000 volts to 1300 volts with the counters properly delayed and set at the proper angle to give a high elastic-event counting rate. It was found that the counting rate was practically independent of the high-voltage settings between 1100 and 1300 volts.

At 2° (lab) at 6.2 Bev the difference in times of flight of protons arriving at the inside telescope was 0.9×10^{-9} second. The cross section was measured with the coincidence circuit resolution time of 6×10^{-9} second. The resolution time was then lengthened to 10^{-8} second so as to determine if the spread in time of flight was causing elastic events to be missed. No increase in the cross section was measured with the lengthened resolution time.

At this angle and energy, it was computed that the inside proton should reach the end counter of the inside telescope with ~ 17 Mev energy. To determine whether any elastic events were being missed because some protons did not have enough energy to reach the last inside counter, the cross section was measured by requiring only a double coincidence between counters No. 1 and No. 3. No increase in the cross section was found over that measured with the normal threefold coincidence.

CHAPTER V

RESULTS

The differential cross sections for elastic proton-proton scattering have been measured by this counter experiment at

0.92 Bev from 91.7° to 49.4°, center-of-mass system

2.24 Bev from 93.5° to 14.8°, center of mass (5° laboratory angle)

3.49 Bev from 78.5° to 34.2°, center of mass

4.40 Bev from 69.0° to 11°, center of mass (3° laboratory angle)

6.2 Bev from 27.6° to 8.3°, center of mass (2° laboratory angle).

An attempt was made to measure the elastic cross section at 6.2 Bev at 8° laboratory angle (32.6° center-of-mass), but the elastically scattered particles were so few as to be obscured by the accidental background. It is interesting to note that the elastic scattering cross section at 6.2 Bev is almost wholly contained within the forward 30° (center-of-mass system).

Preliminary results of the cross-section angular distribution at large angles (c.m.) have been published [14]. More complete and accurate values for $\frac{d\sigma'}{d\Omega'}$ at these large angles (c.m.) are:

Energy (Bev)	Angle, center-of-mass (degrees)	$\frac{d\sigma'}{d\Omega'}$ (mb/sterad)
2.24	23.4	12.1
	29.2	7.7
	44.0	1.5
	57.6	0.58
	70.3	0.33
	93.5	0.19
3.49	34.2	1.7
	49.2	0.26
	64.4	0.07
	78.5	0.06

Energy (Bev)	Angle, center-of-mass (degrees)	$\frac{d\sigma'}{d\Omega'}$ (mb/sterad)
4.40	17.5	15.6
	28.5	2.6
	35.4	0.54
	37.5	0.61
	53.2	0.12
	69.2	0.045

The error in the absolute values for $\frac{d\sigma'}{d\Omega'}$ is about ± 20%. This error is almost entirely due to errors associated with the monitor telescope calibration, the induction-electrode calibration, and the interpretation of the shape of the curve of counting rate versus inside telescope position. The error in the relative values of $\frac{d\sigma'}{d\Omega'}$ at the various angles is much less, about 8%, and depends on the counting statistics.

The data for the cross-section measurements at small angles (c.m.) are being analyzed and are to be published in the near future. Preliminary results indicate that the differential cross section for elastic proton-proton scattering becomes more sharply peaked at small angles (c.m.) as the energy increases in the range of this experiment (0.92 to 6.2 Bev).

APPENDIX

PROTON-PROTON SCATTERING: KINEMATICAL EQUATIONS

Equations frequently used in proton-proton scattering at relativistic velocities are presented here for convenient reference. Beginning with basic relativistic definitions and relations, the scattering-problem equations are developed in a convenient form.

Consider two particles of relativistic mass m_1, m_2, velocities v_1, v_2, in the laboratory system; relativistic mass m_1', m_2', velocities v_1', v_2' in the center-of-mass system, with the moving reference plane the center-of-mass system, moving with velocity u. Center-of-mass quantities are designated with a prime.

Define the relativistic ratio

$$\beta_1 = \frac{v_1}{c} \; ; \; \beta_x = \frac{v_x}{c} \; ; \; \beta' = \frac{v'}{c} \; ; \; \beta_c = \frac{u}{c} \text{ , etc.,} \tag{A-1}$$

where c is the velocity of light.

Define

$$\gamma_x = \frac{1}{\sqrt{1 - \beta_x^2}} \; ; \; \gamma' = \frac{1}{\sqrt{1 - \beta'^2}} \; ; \; \gamma_c = \frac{1}{\sqrt{1 - \beta_c^2}} \text{ , etc.} \tag{A-2}$$

The well-known relation between the velocities in the fixed laboratory system and the velocities in the moving system (center-of-mass system) is

$$v_x = \frac{v_x' + u}{1 + \frac{v_x' u}{c^2}} \quad \text{or} \quad \beta_x = \frac{\beta_x' + \beta_c}{1 + \beta_x' \beta_c} \; . \tag{A-3}$$

Here the velocity of the center of mass is assumed to be in the x direction.

We have

$$v_y = \frac{v_y'}{\gamma_c \left(1 + \frac{v_x' u}{c^2}\right)} \quad \text{or} \quad \beta_y = \frac{\beta_y'}{\gamma_c (1 + \beta_x' \beta_c)} \; , \tag{A-4}$$

$$v'_x = \frac{v_x - u}{1 - \frac{v_x u}{c^2}} \quad \text{or} \quad \beta'_x = \frac{\beta_x - \beta_c}{1 - \beta_x \beta_c}\,, \tag{A-5}$$

$$v'_y = \frac{v_y}{\gamma_c \left(1 - \frac{v_x u}{c^2}\right)} \quad \text{or} \quad \beta'_y = \frac{\beta_y}{\gamma_c (1 - \beta_x \beta_c)}\,. \tag{A-6}$$

The relativistic mass equations are

$$m_1 = m_{10}\,\gamma_x \quad ; \quad m'_1 = m_{10}\,\gamma'_x, \tag{A-7}$$

where m_{10} is the rest mass of Particle 1, etc.

The relativistic momentum multiplied by c is

$$p_{1x}\,c = m_1\,v_x\,c = m_1\,c^2\,\beta_x = m_{10}\,c^2\,\gamma_x\,\beta_x$$

$$\text{and} \quad p'_{1x}\,c = m_{10}\,c^2\,\gamma'_x\,\beta'_x. \tag{A-8}$$

The total energy of a relativistic particle is

$$E_1 = m_1\,c^2 = m_{10}\,\gamma_x\,c^2,$$

$$E'_1 = m'_1\,c^2 = m_{10}\,\gamma'_x\,c^2. \tag{A-9}$$

When β is eliminated in Eqs. (A-8) and (A-9) another expression for the energy is obtained

$$E_1^{\,2} = p_{1x}^{\,2}\,c^2 + (m_{10}\,c^2)^2\,. \tag{A-10}$$

To obtain an expression for γ_x in terms of center-of-mass quantities, combine Eqs. (A-2) and (A-3):

$$\gamma_x = \frac{1}{\sqrt{1 - \left(\frac{\beta'_x + \beta_c}{1 + \beta'_x \beta_c}\right)^2}} = \frac{1 + \beta'_x\,\beta_c}{\sqrt{(1 - \beta_c^2)(1 - \beta_x^2)}} = (1 + \beta'_x\,\beta_c)\gamma'_x\gamma_c. \tag{A-11}$$

Similarly, from Eqs. (A-2) and (A-5), obtain

$$\gamma'_x = (1 - \beta_x \beta_c) \gamma_c \gamma_x. \tag{A-12}$$

Multiplying Eqs. (A-3) and (A-11), we have

$$\beta_x \gamma_x = (\beta'_x + \beta_c) \gamma_c \gamma'_x . \tag{A-13}$$

Multiplying Eqs. (A-5) and (A-12), we obtain

$$\beta'_x \gamma'_x = (\beta_x - \beta_c) \gamma_c \gamma'_x . \tag{A-14}$$

If both particles are of equal rest mass, i.e., $m_{10} = m_{20}$, then in the center-of-mass system we have

$$v'_1 = -v'_2,$$

$$\beta'_{1x} = -\beta'_{2x},$$

$$\gamma'_{1x} = \gamma'_{2x} \tag{A-15}$$

The total energy of the center-of-mass system, U', where the two particles are considered to move along with the velocity of the center of mass, is

$$U' = m_{10} \gamma_c c^2 + m_{20} \gamma_c c^2 = 2 m_{10} c^2 \gamma_c \tag{A-16}$$

If the energy of each particle is considered separately in the center-of-mass system, the total energy U' is also

$$U' = m_{10} \gamma'_1 c^2 + m_{20} \gamma'_2 c^2 = 2m_{10} \gamma'_1 c^2; \tag{A-17}$$

from Eqs. (A-16) and (A-17), $\gamma_c = \gamma'_1$,

$$\beta_c = \beta'_1,$$

$$u = v'_1. \tag{A-18}$$

If we make use of (A-18), Eq. (A-3) becomes

$$v_x = \frac{2u}{1 + \frac{u^2}{c^2}} \quad \text{or} \quad \beta_x = \frac{2\beta_c}{1 + \beta_c^2} \tag{A-19}$$

Similarly, Eq. (A-11) becomes

$$\gamma_x = (1 + \beta_c^2)\, \gamma_c^2, \tag{A-20}$$

and Eq. (A-13) becomes

$$\beta_x\, \gamma_x = 2\, \beta_c\, \gamma_c^2 \;. \tag{A-21}$$

In the laboratory system the total energy of both protons, U, is

$$U = m_1\, c^2 + m_2\, c^2,$$

and where $m_{10} = m_{20}$ and m_{20} is at rest in the laboratory system,

$$U = m_{10}\, \gamma_x\, c^2 + m_{20}\, c^2 = m_{10}\, c^2\, (\gamma_x + 1). \tag{A-22}$$

Substituting into Eq. (A-22) the value of γ_x in Eq. (A-20), we have

$$U = m_{10}\, c^2 \left[(1 + \beta_c^2)\, \gamma_c^2 + 1\right] = m_{10}\, c^2 \left[\frac{1 + \beta_c^2}{1 - \beta_c^2} + 1\right]$$

$$= m_{10}\, c^2 \left[\frac{2}{1 - \beta_c^2}\right] = 2\, m_{10}\, c^2\, \gamma_c^2 = 2\, m_1'\, c^2\, \gamma_c; \tag{A-23}$$

from Eq. (A-16), where $U' = 2\, m_1'\, c^2$, we obtain

$$U = \gamma_c\, U', \tag{A-24}$$

which is a convenient relation between the energy in the laboratory system and the energy in the center-of-mass system.

The total momentum in the laboratory system is

$$p = p_1 + p_2 = m_1\, v_{1x} + m_2\, v_{2x} = m_1\, v_{1x},$$

since $v_2 = 0$.

From Eqs. (A-8), (A-16), and (A-21) the total laboratory momentum multiplied by c is found to be

$$p\,c = m_{10}\,c^2\,\gamma_x\,\beta_x = 2m_{10}\,c^2\,\beta_c\,\gamma_c^2 = U'\,\beta_c\,\gamma_c;$$

now, substituting from Eq. (A-24) for $\gamma_c\,U'$, we obtain

$$p\,c = \beta_c\,U. \tag{A-25}$$

Re-written, it is

$$\beta_c = \frac{p\,c}{U}\,, \tag{A-26}$$

which gives us an expression for β_c of the center of mass in terms of the laboratory momentum and energy.

The equations for proton-proton scattering reduce to a simplified form when the nuclear rest mass is taken as the unit of energy. (One nuclear rest mass = 0.938 Bev.)

If, then, we have $m_{10}c^2 = 1$, Eq. (A-22) for the total energy U in the laboratory system becomes

$$U = m_1\,c^2 + m_{20}\,c^2 = E + 1, \tag{A-27}$$

where E is the energy of the incident proton in nuclear mass units; from Eq. (A-7), where $E^2 = p^2\,c^2 + m_{10}^2\,c^4$, we rewrite

$$p\,c = \sqrt{E^2 - 1}. \tag{A-28}$$

Equation (A-26) now is

$$\beta_c = \frac{p\,c}{U} = \frac{\sqrt{E^2 - 1}}{E + 1} = \sqrt{\frac{E - 1}{E + 1}} = \sqrt{\frac{U - 2}{U}}\ . \tag{A-29}$$

From Eqs. (A-2) and (A-29), we have

$$\gamma_c = \frac{1}{\sqrt{1 - \beta_c^2}} = \frac{1}{\sqrt{1 - \frac{E - 1}{E + 1}}} = \sqrt{\frac{E + 1}{2}} = \sqrt{\frac{U}{2}}\ . \tag{A-30}$$

From Eqs. (A-29) and (A-30),

$$\beta_c \, \gamma_c = \sqrt{\frac{E-1}{2}} = \sqrt{\frac{U-2}{2}} \quad . \tag{A-31}$$

Equation (A-16) $U' = 2m_{10}\, c^2\, \gamma_c$ becomes

$$U' = 2\gamma_c = \sqrt{2(E+1)} = \sqrt{2\,U} \; . \tag{A-32}$$

In the center-of-mass system we have $U' = E_1' + E_2'$ and $E_1' = E_2'$,

therefore $$E_1' = \frac{U'}{2} = \frac{\sqrt{2U}}{2} = \sqrt{\frac{U}{2}} \; . \tag{A-33}$$

The properties of the particles after scattering--such as the relativistic mass, energy, momentum, etc.--are denoted with an asterisk (*); e.g., m_1^* , E_1^*, $E_1'^*$, denote relativistic mass and energy of Particle 1, laboratory system, and energy of Particle 1, center-of-mass system, respectively, after scattering. The angle of recoil of the proton scattered through the smaller angle is denoted θ_0 and θ_0' in the laboratory and center-of-mass systems respectively. The angle of recoil of the proton scattered through the larger angle is denoted θ_i or θ_i' .

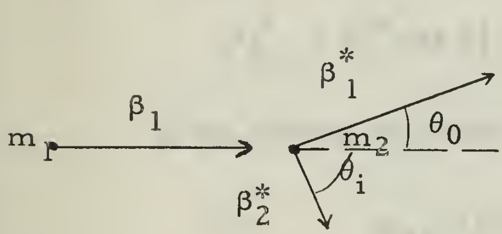

Laboratory system

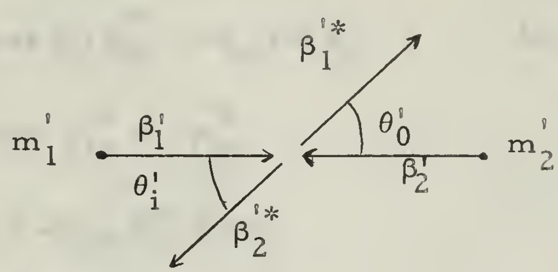

Center-of-mass system

After an elastic collision, the momentum of the two particles is still equal, therefore $\beta_1'^* = \beta_2'^*$.

The energy in the center-of-mass system remains the same:

$$2m_{10}\,\gamma_c\,c^2 = 2m_{10}\,\gamma_1'^*\,c^2;$$

Therefore $$\beta_c = \beta_1'^* = -\beta_2'^* \qquad \text{(A-34)}$$

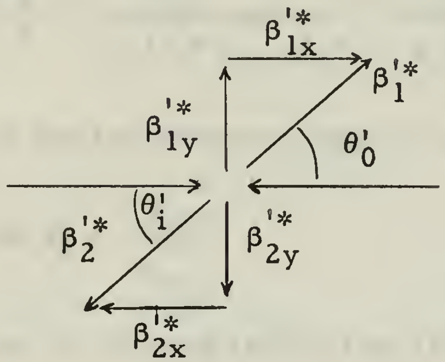

As indicated in the sketch above

$$\beta_{1x}'^* = \beta_1'^* \cos\theta_0' = \beta_c \cos\theta_0';\ \beta_{1y}'^* = \beta_c \sin\theta_0', \qquad \text{(A-35)}$$

$$\beta_{2x}'^* = \beta_2'^* \cos\theta_i' = -\beta_c \cos\theta_i';\ \beta_{2y}'^* = -\beta_c \sin\theta_i'. \qquad \text{(A-36)}$$

In an elastic collision, we have $p_{1y}'^* = -p_{2y}'^*$

or $$m_{10}\,\beta_1'^* \sin\theta_0 = -m_{20}\,\beta_2'^* \sin\theta_i,$$

but $m_{10} = m_{20}$ and $\beta_1'^* = -\beta_2'^*$;

therefore $$\theta_0' = \theta_i'$$

and so Eq. (A-36) becomes

$$\beta_{2x}'^* = -\beta_c \cos\theta_0';\quad \beta_{2y}'^* = -\beta_c \sin\theta_0'. \qquad \text{(A-37)}$$

In the laboratory system after collision, from Eqs. (A-3) and (A-35), we have

$$\beta_{1x}^{*} = \frac{\beta_{1x}^{'*} + \beta_c}{1 + \beta_{1x}^{'*}\beta_c} = \frac{\beta_c \cos\theta_0' + \beta_c}{1 + \beta_c^2 \cos\theta_0'} = \frac{\beta_c(1 + \cos\theta_0')}{1 + \beta_c^2 \cos\theta_0'} . \qquad \text{(A-38)}$$

From Eqs. (A-4) and (A-35),

$$\beta_{1y}^{*} = \frac{\beta_{1y}^{'*}}{\gamma_c(1 + \beta_{1x}^{'*}\beta_c)} = \frac{\beta_c \sin\theta_0}{\gamma_c(1 + \beta_c^2 \cos\theta_0')} \qquad \text{(A-39)}$$

The angle θ_0 in the laboratory system is defined by

$$\tan\theta_0 = \frac{\beta_{1y}^{*}}{\beta_{1x}^{*}} . \qquad \text{(A-40)}$$

Substituting Eqs. (A-38) and (A-39) into (A-40), we obtain

$$\tan\theta_0 = \frac{\beta_c \sin\theta_0'}{\gamma_c(1 + \cos\theta_0')} = \frac{2\sin\frac{\theta_0'}{2}\cos\frac{\theta_0'}{2}}{\gamma_c\left(2\cos^2\frac{\theta_0'}{2}\right)} = \frac{\sin\frac{\theta_0'}{2}}{\gamma\cos\frac{\theta_0'}{2}} ,$$

therefore $$\tan\theta_0 = \frac{\tan\frac{\theta_0'}{2}}{\gamma_c} = \sqrt{\frac{2}{E+1}}\,\tan\frac{\theta_0'}{2} . \qquad \text{(A-41)}$$

From Eqs. (A-3) and (A-37),

$$\beta_{2x}^{*} = \frac{\beta_{2x}^{'*} + \beta_c}{1 - \beta_{2x}^{'*}\beta_c} = \frac{\beta_c(1 - \cos\theta_0')}{1 - \beta_c^2 \cos\theta_0'} . \qquad \text{(A-42)}$$

Combining Eqs. (A-4) and (A-37), we obtain

$$\beta_{2y}^{*} = \frac{\beta_{2y}^{'*}}{\gamma_c(1 + \beta_{2y}^{'*}\beta_c)} = \frac{-\beta_c \sin\theta_0'}{\gamma_c(1 - \beta_c^2 \cos\theta_0')} \qquad \text{(A-43)}$$

θ_i is defined by

$$\tan \theta_i = \frac{\beta^*_{2y}}{\beta^*_{2x}} . \tag{A-44}$$

Substituting from Eq. (A-42) and Eq. (A-43), we get

$$\tan \theta_i = \frac{-\sin \theta_0'}{\gamma_c (1 - \cos \theta_0')} = \frac{-2 \sin \frac{\theta_0'}{2} \cos \frac{\theta_0}{2}}{\gamma_c (2 \sin^2 \frac{\theta_0'}{2})} = \frac{-\cos \frac{\theta_0'}{2}}{\gamma_c \sin \frac{\theta_0'}{2}}$$

$$= \frac{\cos \frac{\theta_0'}{2}}{\gamma_c \sin \frac{\theta_0'}{2}} ,$$

therefore $$\tan \theta_i = \frac{1}{\gamma_c \tan \frac{\theta_0'}{2}} = \sqrt{\frac{2}{E + 1}} \frac{1}{\tan \frac{\theta_0'}{2}} . \tag{A-45}$$

We multiply Eq. (A-41) by (A-45) to obtain the following relation between θ_0 and θ_i:

$$\tan \theta_0 \tan \theta_i = \frac{1}{\gamma_c^2} = \frac{2}{E + 1} = \frac{2}{U} . \tag{A-46}$$

The energy of the scattered protons is

$$E^*_{1,2} = m^*_{1,2} c^2 = m_{10} \gamma^*_{1,2} c^2 . \tag{A-47}$$

In general, if we have $v^2 = v_x^2 + v_y^2$, Eq. (A-2) can be written

$$\gamma = \frac{1}{\sqrt{1 - \beta^2}} = \frac{1}{\sqrt{1 - (\beta_x^2 + \beta_y^2)}}$$

$$\text{or} \qquad \gamma_1^* = \frac{1}{\sqrt{1 - (\beta^{*2}_{1x} + \beta^{*2}_{1y})}} . \tag{A-48}$$

Substituting Eqs. (A-38) and (A-39) into (A-48), we obtain

$$\gamma_1^* = \sqrt{1 - \frac{\beta_c^2 (1 + \cos \theta_0')^2}{(1 + \beta_c^2 \cos \theta_0')^2} - \frac{\beta_c^2 \sin^2 \theta_0'}{\gamma_c^2 (1 + \beta_c^2 \cos \theta_0')^2}}$$

$$= \frac{1 + \beta_c^2 \cos \theta_0'}{\sqrt{(1 + \beta_c^2 \cos \theta_0')^2 - \beta_c^2 (1 + \cos \theta_0')^2 - \frac{\beta_c^2}{\gamma_c} \sin^2 \theta_0'}},$$

$$\gamma_1^* = \frac{1 + \beta_c^2 \cos \theta_0'}{\sqrt{1 - 2\beta_c^2 + \beta_c^4}} = \frac{1 + \beta_c^2 \cos \theta_0'}{1 - \beta_c^2} = (1 + \beta_c^2 \cos \theta_0') \gamma_c^2. \quad \text{(A-49)}$$

Similarly, using Eqs. (A-42) and (A-43),

$$\gamma_2^* = (1 - \beta_c \cos \theta_0') \gamma_c^2. \quad \text{(A-50)}$$

Equation (A-47) then becomes

$$E_{1,2}^* = m_{10} c^2 (1 \pm \beta_c \cos \theta_0') \gamma_c^2, \quad \text{(A-51)}$$

rewritten $E_{1,2}^* = E_1' \gamma_c (1 \pm \beta_c^2 \cos \theta_0')$

$$= \frac{E + 1}{2} \left(1 \pm \frac{E - 1}{E + 1} \cos \theta_0'\right) \quad \text{(A-52)}$$

For any given θ_0 or θ_i, θ_0' is determined by Eq. (A-41) or (A-45) for the particular energy of the incident proton. The energy of the scattered proton observed at any θ_0 or θ_i may then be determined with Eq. (A-52) above.

With $E_{1,2}^*$ known, the kinetic energy $T_{1,2}^*$ is found from

$$T_{1,2}^* = E_{1,2}^* - 1. \quad \text{(A-53)}$$

[illegible]

$$[illegible]$$

$$[illegible]$$

[illegible]

$$[illegible]$$

[illegible]

$$[illegible]$$

[illegible]

$$[illegible]$$

[illegible]

[illegible]

The momentum multiplied by c of the recoiling nucleon is from Eq. (A-7):

$$p_{1,2}^{*}c = \sqrt{E_{1,2}^{*2} - 1} \tag{A-54}$$

The β of the recoiling nucleon is

$$\beta_{1,2}^{*} = \frac{v_{1,2}^{*}}{c} = \frac{m_{1,2}\, v_{1,2}^{*}\, c}{m_{1,2}\, c^{2}} = \frac{p_{1,2}^{*}\, c}{E_{1,2}^{*}} = \frac{\sqrt{E_{1,2}^{*2} - 1}}{E_{1,2}^{*}} \, . \tag{A-55}$$

BIBLIOGRAPHY

1. Chamberlain, Segrè, and Wiegand	Physical Review, Vol. 83, p 923, 1951
2. Oxley and Schamberger	Physical Review, Vol. 85, p 416, 1952
3. Tower, O. A.,	Physical Review, Vol. 85, p 1024, 1952
4. Cassels, Pickavance, and Stafford	Proceedings of the Royal Society (London) Vol. 214, p 262, 1952
5. Marshall, Marshall, and Nedzel	Physical Review, Vol. 92, p 834, 1953
6. Chamberlain, Pettengill, Segrè, and Wiegand	Physical Review, Vol. 93, p 1424, 1954
7. Kruse, Teem, and Ramsey	Physical Review, Vol. 94, p 1795, 1954
8. Sutton, Fields, Fox, Kane, Mott, and Stallwood	Physical Review, Vol. 97, p 783, 1955
9. Smith, McReynolds, and Snow	Physical Review, Vol. 97, p 1186 (L), 1955
10. Vecksler, V.	Journal of Physics, USSR, Vol. 9, p 153, 1945
11. McMillan, E. M.	Physical Review, Vol. 68, p 143, 1945
12. Chupp, Murray, and Wenzel	UCRL-3420, Feb. 1956
13. McMillan, E. M.	Review of Scientific Instruments, Vol. 22, p 117, 1951
14. Cork, Bruce and Wenzel, ~~Joseph H.~~ Wm. A.	Physical Review, Vol. 100, p 962(A), 1955

28082

Thesis
C338

Causey
Description of a counter experiment to measure the elastic proton-proton scattering cross section at bevatron energies.